# MEG Tomography of Human Cortex and Brainstem Activity in Waking and REM Sleep Saccades

Andreas A. Ioannides[1], Maria Corsi-Cabrera[2], Peter B.C. Fenwick[1], Yolanda del Rio Portilla[1,2], Nikos A. Laskaris[1], Ara Khurshudyan[1], Dionyssios Theofilou[1,3], Tadahiko Shibata[1], Sunao Uchida[4], Tetsuo Nakabayashi[4] and George K. Kostopoulos[3]

[1]Laboratory for Human Brain Dynamics, RIKEN Brain Science Institute (BSI), 2-1 Hirosawa, Wako-shi, Saitama, 351-0198, Japan, [2]Facultad de Psicologia, Posgrado, Universidad Nacional Autónoma de México, México City, México, [3]Department of Physiology, Medical School, University of Patras, Patras, Greece and [4]Department of Sleep Disorders Research, Tokyo Institute of Psychiatry, Tokyo 156-8585, Japan

**We recorded the magnetoencephalographic (MEG) signal from three subjects before, during and after eye movements cued to a tone, self-paced, awake and during rapid eye movement (REM) sleep. During sleep we recorded the MEG signal throughout the night together with electroencephalographic (EEG) and electromyographic (EMG) channels to construct a hypnogram. While awake, just prior to and during eye movements, the expected well time-locked physiological activations were imaged in pontine regions, with early 3 s priming. Activity in the frontal eye fields (FEF) was identified in the 300 ms before the saccade onset. Visual cortex activation occurred 200 ms after saccades. During REM, compared to the eyes closed awake condition, activity was higher in supplementary motor area (SMA) and lower in inferior parietal and precuneus cortex. Electro-occulographic (EOG) activity just prior to REM saccades correlated with bilateral pontine and FEF activity some 250–400 ms before REM saccade onset, which in turn was preceded 200 ms earlier by reciprocal activation of the pons and FEF. An orbitofrontal-amygdalo-parahippocampal-pontine sequence, possibly related to emotional activation during REM sleep, was identified in the last 100 ms leading to the REM saccade, but not linked to saccade initiation.**

## Introduction

As the name implies, one of the most salient features of rapid eye movement sleep (REM) are the rapid eye movement saccades (REMS). Apart from some small differences in velocity REMS share with saccadic eye movements of wakefulness the main characteristic, the ballistic nature (Takahashi and Atsumi, 1997). Neurophysiological mechanisms controlling REM sleep have been mainly studied in cats, where specific cholinergic mesopontine nuclei in peribrachial areas have been identified as important for REM sleep and ponto-geniculo-occipital (PGO) wave generation (Datta and Hobson, 1994). Data from cortical lesions in man (Jouvet *et al.*, 1961), and from decortication and pontine transections in cats (Jouvet, 1962) show that PGOs and REM can be triggered by pontine mechanisms without the participation of the cortex. These findings together with the close temporal relationship between PGOs and REMS (Cespuglio *et al.*, 1975) and neurophysiological and neurochemical manipulations at the level of the caudoventral pontine tegmentum (Vanni-Mercier and Debilly, 1998) suggest a primarily bottom-up influence (Hobson *et al.*, 1998), possibly based on a common structure.

Studies of the central mechanisms underlying purposeful waking saccades in primates have identified cortical and subcortical parallel networks converging onto brain stem nuclei as the final output to initiate eye movements (Leigh and Zee, 1999). These studies have demonstrated that in the awake state motor commands can be initiated either from the superior colliculi (Moschovakis and Highstein, 1994) or, for intentional saccades, from the cortex, i.e. the frontal eye fields (FEFs) (Schall, 1991; Segraves and Park, 1993; Tehovnik *et al.*, 2000). For horizontal eye movement, these commands modulate the para-median pontine reticular formation, the horizontal gaze center, while vertical movements depend on the more rostral interstitial nucleus of the medial longitudinal fasciculus, the vertical gaze center. For horizontal movements, reciprocal innervations of the lateral rectus of one eye and medial rectus of the other ensure conjugate saccades to one side. For upward and downward saccades inhibitory and excitatory activity is in the mesencephalic vertical gaze centers which are activated similarly on both sides of the brainstem (Leigh and Zee, 1999).

In humans, more recent imaging studies by both PET and fMRI have shown that waking eye movement is associated with activation of FEFs and thalamic, putamen and cerebellar structures (O'Sullivan *et al.*, 1995; Petit *et al.*, 1996; Bodis-Wollner *et al.*, 1997; Luna *et al.*, 1998). For REMS, the few neuroimaging studies in humans have shown a correlation between the number of REMS and the metabolic activity in the same cortical areas, which are involved in waking eye movements (Hong *et al.*, 1995), and in brain regions where PGOs have been recorded in animals (Peigneux *et al.*, 2001). All PET studies during REM sleep in humans have shown activation of the limbic system (Maquet *et al.*, 1996; Nofzinger *et al.*, 1997; Braun *et al.*, 1998). These studies have produced useful information but they do not distinguish between tonic or persistent activations and phasic activations temporally related to the preparation and execution of eye movement.

There is previous evidence for strong magnetoencephalographic (MEG) signals generated by brainstem regions in the porcine preparation (Hashimoto *et al.*, 1996). So, we hypothesized that electrical events in the brainstem related to saccades will produce measurable MEG signal time-locked with saccade onset defined by the electro-oculogram (EOG). Tomographic estimates of activity can then be computed from the MEG signal using magnetic field tomography (MFT) (Ioannides *et al.*, 1990). Predictions about the pontine current flow for each saccade direction can be made from the sequence of activations in the gaze control centers identified in animals (Segraves and Park, 1993). For example, before the onset of horizontal saccades the pontine current flow should reverse in the midline of the brain stem. The entire pattern should have opposite polarity for saccades to the left and right and in each case it should reverse after saccade onset. These predictions contrasted with the MFT solutions allow us to test whether brainstem activity can be

detected, sized and possibly imaged, and if so how well events can be separated on either side of the brainstem.

The onset of eye movement can be estimated from the EOG and used to average single trials in a given direction. Around saccade onset, the amplitude of the average EOG for 10–20 trials is ~10 times higher than the background. In the single trial EOG signal the ratio of any one peak to the others or to the peristimulus period is well below 10, because of the ever-present ocular muscle activity. In the corresponding case of limb movements, similar electromyographic (EMG) activity reflects a linkage between the motor cortex and spinal motor neuron pool (Conway *et al.*, 1995), and it was used to demonstrate a correlation between the corticomuscular phase synchronization and the time course of both M1 and EMG signals (Gross *et al.*, 2000). We anticipated a similar relationship between ocular muscle activity and distant regional brain activity. If eye movement or ocular EMG transients in the EOG express even weakly the programming of eye movements from cortical and pontine centers, then activity from the cortex and the pontine nuclei can be disentangled in relation to initiation, maintenance and stopping of eye movement.

### *Aim of the Study*

Our study tests the following hypotheses. (i) Brainstem and cortical activity related to eye movements could be imaged while waking and sleeping. If (i) was correct then the following would be tested. (ii) Awake, horizontal and vertical eye movement will show different patterns of activation in the brain stem but will broadly follow the known physiology. (iii) REMS will have primarily a pontine generator with characteristic limbic activation.

## Materials and Methods

### *General Experimental Methods*

For this study we used data from three male, right-handed, drug-free subjects (aged 25, 30 and 31 years old) with regular sleep habits (as assessed by questionnaires and interview). All three subjects had normal or corrected acuity, normal eye movements and were free of neuropsychiatric illness and all medication. Data from a pilot run (fourth subject) produced similar results but they were not used because of slight differences in recording parameters. The RIKEN ethical committee approved the protocol. After subject selection the protocol and the experiment were explained and informed consent was obtained. All subjects slept in the laboratory for two consecutive nights; the first for adaptation to the experimental conditions and the second for polysomnography and data acquisition.

On the first evening (adaptation night) the subject was trained for eye movements in the preparation room. The head shape was digitized together with head coils used later for identifying the head position relative to the MEG sensors. Finally, EOG and ECG (electrocardiogram) electrodes were attached before the subject was taken to the shielded MEG recording room. The MEG signal was recorded simultaneously with the horizontal (EOG-H) and vertical (EOG-V) EOG channels. The subject returned to the preparation room to sleep on a replica of the MEG bed with the head in a replica of the MEG helmet. Since no polysomnographic data were recorded, the evaluation of the adaptation night sleep as normal is qualified by its reliance on the subjective nature of the reports from each subject.

During the second day the subject worked as usual with the instruction to stay awake throughout the day. He returned to the laboratory after work, had an evening meal and was prepared for MEG recording exactly as for the previous night except for the addition of three extra EEG channels. These were C3 and C4 referenced to A1 and chin electrodes to record the EMG used for sleep scoring. The EOGs were calibrated using controlled eye movements in the MEG room, before the sleep recordings. A preliminary 'on the fly' scoring of the sleep stages was kept. The entire night's MEG signal was recorded for each of the three subjects with no complications.

### *Sleep and Sleep Staging*

The data were scored offline by two sleep experts. The two independent scores were compared, a common one agreed and the night hypnogram constructed. Sleep stages were noted according to the standardized manual (Rechtschaffen and Kales, 1968), (W = wake state, MT = subject moving in bed, St.1–St.4 = first to fourth sleep stages, REM = REM sleep stage). Standard indicators identified REM: desynchronized EEG, minimization of muscle tone and the emergence of REMS. Figure 1 shows typical examples of a hypnogram, EEG and MEG channels.

Despite a slight reduction in total sleep time (mean: 369.33 min, SD 41.52 min; efficiency index 0.79) the percentage of REM sleep (mean 26.24, SD 11.07) and the latency to REM sleep (85.33, 25.77) were within normal ranges for young adults (Williams *et al.*, 1974). Although stage 3 and 4 were slightly lower and stage 1 slightly higher than normal, for each subject all sleep stages were in broadly the expected sequence: stage 1 (mean = 15.06, SD = 3.75), stage 2 (46.12, 6.6), stages 3 and 4 (12.62, 4.34). The hypnograms were judged qualitatively physiological, a fact corroborated by the subjects report of restful sleep similar to their average night. All subjects completed a debriefing questionnaire and scored their sleep in different aspects compared to their average sleep. The average scores for the three subjects for the sleep during the recording night was overall quality (87%), refreshing (70%) and of normal depth (80%). Based on the subjects' own evaluation the sleep during the recording night was judged better than during the adaptation night (68, 53 and 63%, respectively).

### *MEG Recordings and Signal Processing*

The MEG data were recorded using the whole-head Omega biomagnetometer (CTF Systems Inc., Vancouver, Canada) inside a $3 \times 4 \times 2.4$ m shielded room (NKK, Kawasaki, Japan). The raw signals from the 151 primary MEG channels, the 28 reference sensors and from auxiliary channels needed for sleep scoring, eye movement and heart monitoring were recorded continuously on a 100 GB disk after low-pass filtering at 208 Hz and digitization at 625 Hz. The continuous recording mode was interrupted every 3 min for head coil localization. The same recording parameters were used for the eye movements during the first night but with head localization only at the beginning and end of each block. Noise runs were also taken before and after each full session (evening).

Two sets of data were derived from the raw signal. The bulk of the analysis was performed after the original signal was digitally high-pass filtered at 0.626 Hz, power-line notch filtered and segmented into epochs, each one lasting from 1 s before to 1 s after the onset of the eye movement. This signal is used for the results displayed in Figures 2, 3 and 5–10. A second version of the data was obtained from the original raw signal via DC-offset removal, low-pass filtering at 20 Hz, down-sampling by 4 and segmentation into 6 s long epochs (3 s on either side of the onset of the eye movement). The average signal for each saccade direction from the first night's recordings was computed and used for source reconstruction. No single trial analysis was performed on this signal. This version was created to study the slow processes without any filtering induced modification of the signal. This analysis eliminated the possibility that the long-lasting priming seen in the averaged epochs was a byproduct of the preprocessing (since the employed high-pass filter belongs to the family of IIR filters). Results using this signal are used only in Figure 4 for analysis and for demonstration in Figure 1.

### *Eye Movements and Single Trial Selection*

Eye movements were recorded under three experimental conditions: on-command saccades (OCS), self-paced saccades (SPS) and REM sleep saccades, or REMS. At the beginning of the first night the subject was trained with a metronome to make well defined OCS and SPS with an inter-saccade period of ~4 s (Fig. 1). A rapid saccade from a central fixation point to the target was required, holding the new position for a second and then returning with a smooth eye movement to the original fixation point. With the subject seated in the dimly illuminated shielded room, the MEG signals were recorded in a separate block for each condition and saccade direction. A block contained 15 saccades in one direction. Saccades of 10° were made from a black fixation cross

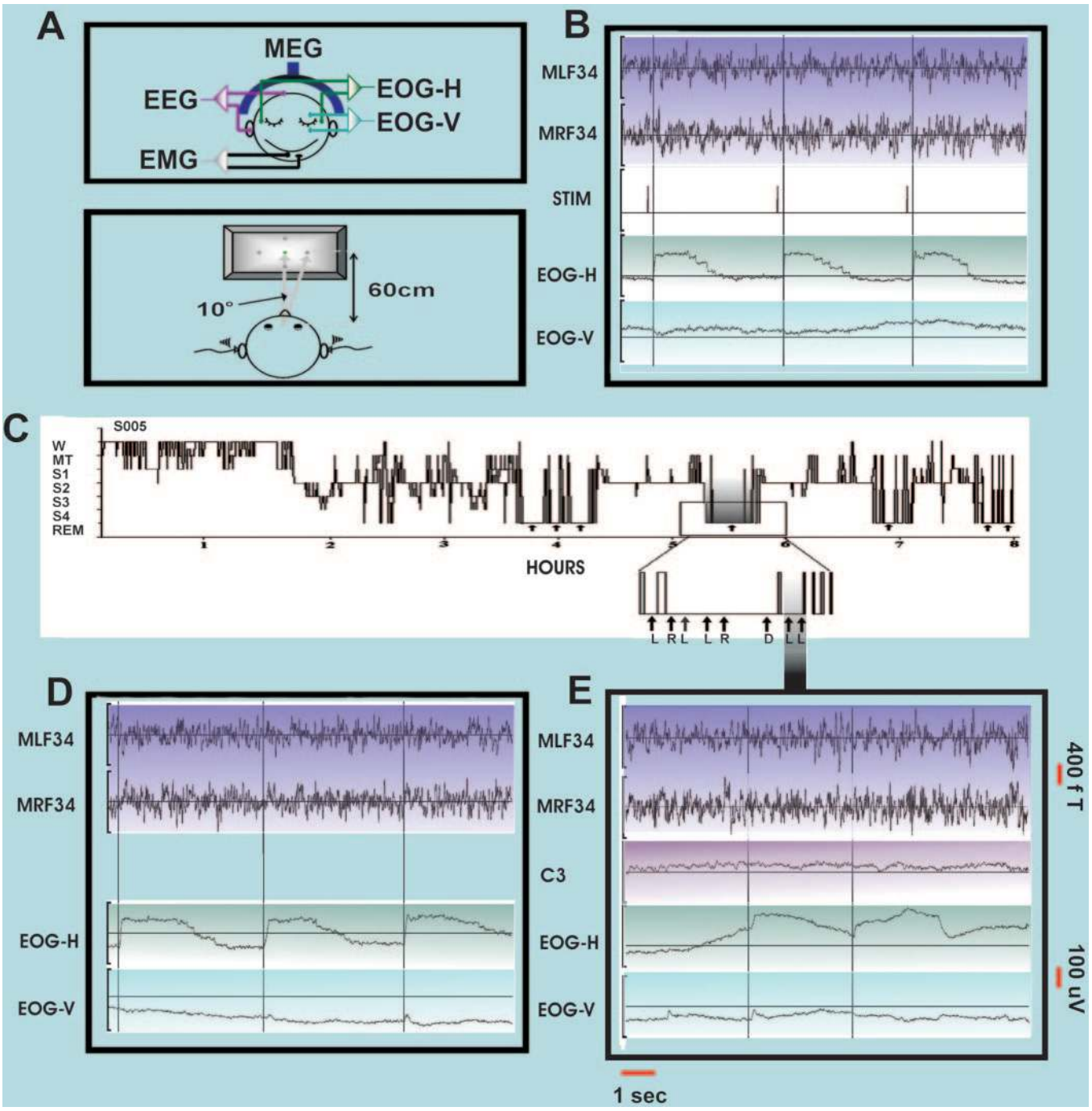


**Figure 1.** (*A*) Schematic diagram of recording arrangements and tasks. (*B*) EOG recording (EOG-H) during OCS, tone recorded on the trigger channel (STIM): leftward saccades is seen on EOG-H to follow the tone onset marked by STIM. Raw MEG signal from magnetometers close to left and right frontal lateral areas show no obvious activity during saccades. (*C*) Hypnogram. W — wake, MT — movement time, S1-4 sleep stages. REMS selected for study (arrows), L — left, R — right, D — down. One REM period from hypnogram expanded to show irregular times of selected left horizontal REMS in *E*. (*D*) MEG and EOG for SPS to the left. (*E*) MEG, EOG and EEG channels for REMS to the left at the times indicated in the hypnogram in *C*. Only REMS with a sharp rise in one direction and a duration comparable to the waking saccades were selected. The time and amplitude scales indicated by bars in *E* apply also to *B* and *D*.

(1.3 cm) located at the center of the screen 60 cm in front of the eyes to a left, right, up or down peripheral target (circle 1.3 cm). In the OCS condition, tones were presented binaurally 4 s apart and subjects were instructed to execute the saccade immediately after the tone. In the SPS condition subjects were asked to execute saccades at the training rate. We limited the number of saccades to ~15 to ensure minimal head movement and because we did not wish to fatigue the subject. Two control conditions were also identified in the MEG recording, the awake state with eyes closed before sleep (ECW) and periods during REM sleep with no eye movement – REM background (REMB).

Precise saccades for each condition and direction were identified and inspected for artefacts. Bad trials were rejected. Particular care was taken to identify pure eye movement trials along the vertical and horizontal axes (referring to the previously calibrated vertical and horizontal EOG records). The all night recording was scored and REMS were extracted from periods between head localizations showing no head

movement. Special attention was paid so that the selected REMS were of pure horizontal (vertical) direction as judged from the EOG, ~10° wide, and had a relative flat baseline. The selected saccades were aligned according to the onset of eye movement using the EOG. Saccade onset was defined by the same expert. For the OCS condition there was a further alignment of the data based on tone onset. Single epochs were selected from ECW and REMB MEG signal segments, free from eye movements (as judged by the EOG trace). The single trials from OCS, SPS and REMS and the single epochs from ECW and REMB were cut to identical length and were pre-processed in identical ways for further analysis.

### *Analysis — Tomographic Reconstructions (MFT)*

Magnetic field tomography (MFT) (Ioannides *et al.*, 1990; Ioannides, 2001) was used to extract estimates for the (non-silent) primary current density vector $\mathbf{J}^p(\mathbf{r},t)$ from the MEG signal, with sensitivity profiles computed from a spherical head model for the conductivity of the head. For each subject and each condition an independent MFT solution was obtained for each time slice of either average or single trial MEG signal. For storage purposes the continuous estimate for $\mathbf{J}^p(\mathbf{r},t)$ was computed at a $17 \times 17 \times 17$ grid points in a box which covered the entire brain, cerebellum and brainstem. Successive time slices were 1.6 ms apart and the grid point separation was ~8.5 mm. Regions of interest (ROIs) were defined either from the average signal at the maximum of MFT solutions or from the statistical analysis of single trial MFT solutions at the loci of significant change in activity. The average time-course of activation along the dominant direction within each ROI, $\bar{J}^p(t)$, was computed from each single trial and average MFT solution. ROIs with consistent time courses of activity across single trials were then selected for further analysis and labeled according to anatomical considerations.

### *Post-MFT Analysis — Statistical Parametric Maps (SPMs)*

Voxel-by-voxel statistical analysis was first performed separately for each subject. The *t*-test was used to compare two distributions, with the element of each distribution made up of the moduli of single trial MFT solutions within well-defined latency windows. For comparisons between two saccade conditions windows centered at the same latency were compared, one from each condition. Statistical comparisons were also made between distributions from an active condition (OCS, SPS or REMS) and distributions from control conditions (ECW and REMB for all latencies and OCS, SPS or REMS at latency period from 900 to 600 ms before saccade onset). We used *t*-test to compute statistical parametric maps (SPM) in much the same way as for PET and fMRI, except that the comparisons were performed over much shorter timescales. Specifically we used active window sizes of 12, 20, 100 and 500 ms and step sizes between successive active windows, of 6, 10, 50 and 250 ms, respectively. Using a set of comparisons avoided the trade off between sensitivity in detecting rapid changes and robustness against loose time locking of events that each single choice entailed. All *P*-values reported include correction for multiple comparisons. Specifically, the conservative Bonferroni-corrected Student's *t*-test is used to minimize alpha inflation due to statistical voxel-by-voxel comparisons.

### *MI Analysis and Influence Diagrams*

Mutual information (MI) was computed between two time-lagged time series (Ioannides *et al.*, 2000). The first time series was always a ROI activation (centered at latency, $t$) and the second was either the activation of another ROI or the EOG signal (centered at, $t + \tau$). Windows of 90 ms (ROI – EOG) and 60 ms (ROI – ROI) were used for MI computations. An isochronous line is defined with unit negative slope so it corresponds to a constant latency of the second ROI (intercept with the horizontal, zero delay axis). An isochronous line in (ROI – EOG) MI maps is named an *iso-ocular line*; it corresponds to EOG activity at a fixed latency, $T_{EOG}$ relative to saccade onset.

Influence diagrams are defined with ROIs arranged in successive rows and time flowing from left to right with arrows defining the linkages between ROIs (read directly from the MI maps). The link of an ROI to the EOG around saccade onset ($T_{EOG} = 0$) is represented according to the timing of the ROI activity: a heavy striped (filled) block is placed on the upper (lower) part of the ROI band if the linked EOG activity is before (after) saccade onset. An influence diagram summarizes in one display many ROI to ROI and ROI to EOG MI maps.

### *Grand Post-SPM and Post-MI analysis*

The SPM data for each subject were first brought into a common Talairach space (Talairach and Tournoux, 1988) and a count was made of the number of subjects satisfying a predefined *P*-value threshold for increases and/or decreases of activity at each voxel for each latency. Inter subject variability in timing (i.e. latency jitter) was allowed only for the narrow (12 ms) windows. The resulting common SPM was then back-transformed to the coordinate system of one subject and overlaid with his MRI for display purposes.

In the case of MI maps, a common threshold across subjects was used after each MI map had been normalized so that the maximum value was 100%. In the results presented in this work the threshold was 30% (OCS, SPS) and 35% (REMS) for MI common across subjects in one condition. For common MI activity across all subjects and more than one condition a 20% threshold was used. Influence diagrams derived from grand post-MI maps summarized in one display large amounts of information regarding functional linkage between areas.

### *Signal-to-noise Ratio (SNR) Measurements*

To quantify the signal content in an ensemble of single trial activation curves we computed their SNR (Raz *et al.*, 1988) using a moving window. The SNR measurement is sensitive to both transient time-locked and phase-reorganization events, provided they emerge coherently across the set of single trial curves. Since, the time-courses for real sources and their ghost images are derived from the same signal, covariation of SNR measures can be used as evidence for ghost sources. The grand SNR, obtained by combining the SNR across subjects and/or different conditions is an objective measure of the time-locked part of the signal.

For additional material describing further details of the measurement and analysis see Supplementary Material.

## Results

### *Eye movements*

The numbers of eye movement and control trials satisfying the selection criteria for each condition and subject are listed in Table 1. The single trials used as controls were selected during quiescent periods for both vertical and horizontal EOG from the ECW and REMB records. The distribution of trials for REMS is very asymmetric and consistently so for all subjects. There is a clear preponderance of saccades to the left. Similar numbers of

**Table 1**
The numbers of eye movement trials satisfying the selection criteria for all subjects and conditions

| | Left | Right | Up | Down |
|---|---|---|---|---|
| S1 | | | | |
| On command | 14 | 14 | 15 | 15 |
| Self-initiated | 13 | 13 | 16 | 12 |
| REM | 16 | 6 | 2 | 4 |
| Eyes closed awake 14 | REMB 30 | | | |
| S2 | | | | |
| On command | 13 | 9 | 6 | 5 |
| Self-initiated | 18 | 14 | 11 | 10 |
| REM | 9 | 4 | 1 | 1 |
| Eyes closed awake 11 | REMB 44 | | | |
| S3 | | | | |
| On command | 15 | 15 | 15 | 14 |
| Self-initiated | 10 | 10 | 10 | 10 |
| REM | 9 | 3 | 2 | 1 |
| Eyes closed awake 20 | REMB 38 | | | |

trials as for the OCS and SPS conditions were obtained from REMS to the left from each subject's entire night recording. Very few REMS satisfied the criteria for the other directions in REM. For OCS and SPS for each subject and condition MFT was applied to average and single trial high-pass filtered at 0.626 Hz (2 s long) MEG signals and to the averaged low-pass filtered below 20 Hz (6 s long) MEG signal. No single trial MFT analysis was performed on the 6 s long data.

### *Brain Stem Activations*

For OCS and SPS the activity in the mid-pontine nuclei (PN) was prominent and easily identified in all three subjects in displays of the instantaneous MFT solutions extracted from the average of each eye movement direction for both the high- and low-pass filtered sets of signals. From the single trial post-reconstruction analysis of the high-pass filtered signal and especially the SPM maps, the same areas could be identified for the same conditions and for the REMS (eye movements to the left only). Figure 2 shows examples of common SPMs for OCS extracted from the 2 s, high-pass filtered MEG signal. The same areas were identified in the analysis of individual subjects for SPS. During SPS, pontine activity was however less rigidly time locked, so latency ranges with common pontine activation were seen to the right for only two subjects while for down, no common period with high SPMs was found across subjects.

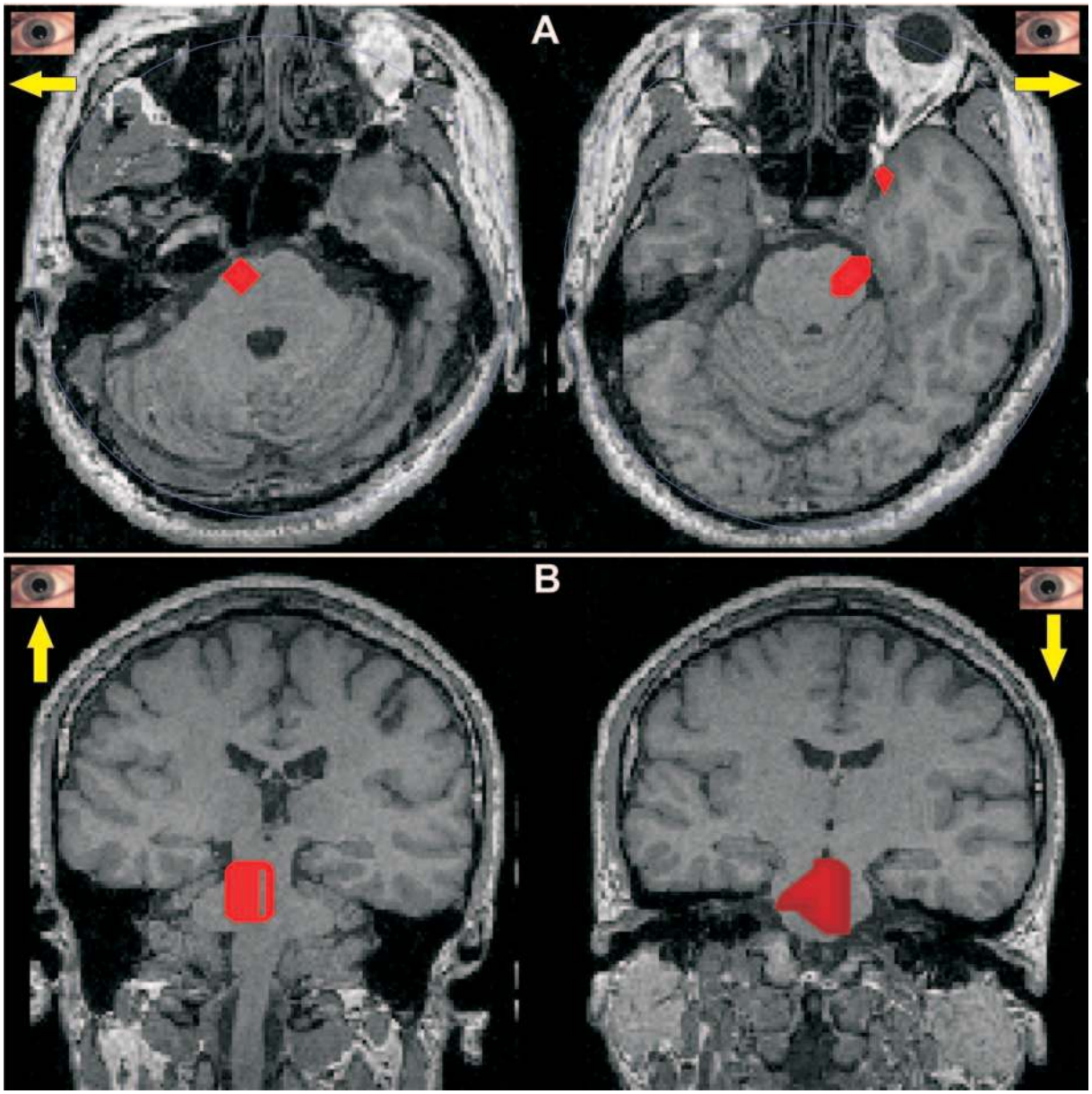


**Figure 2.** SPMs for OCS condition showing common activations in the brain stem for the 100 ms period just before saccades. In each case the SPMs were computed for each subject separately by comparing the moduli of the current density in the 100 ms leading to the saccade with the corresponding distributions in the far prestimulus period (–900 to –600 ms). The results were then transformed to the Talairach space and common activations across subjects identified for each voxel. The results were then backtransformed to the MRI of one of the subjects for display. (*A*) shows the SPMs for horizontal eye movements (move left on left and move right on right) and (*B*) shows the SPMs for vertical eye movement (move up on left and move down on right). The red area corresponds to voxels of common statistically significant increase ($P < 0.05$) for all three subjects in the first three directions, but for only two subjects in OCS-down (S1 and S3), possibly because for OCS down subject S2 produced fewer saccades satisfying the selection criteria.

The time-courses of pontine activations were computed from the MFT solutions, using the same ROI definition for each subject across conditions and eye movement direction. Figure 3 shows, for saccades to the left, the average time course of activation for ROIs placed on the PN gaze center for all three subjects and all three active conditions (OCS, SPS and REMS). For each ROI the average across single trials was computed for each subject and condition directly from the corresponding single trial MFT solution. This tedious way of computing the average PN activation was necessary for REMS because different single trials corresponded to different times during the night and hence different head positions relative to the sensors. It was also used for OCS and SPS to maintain consistency in the computations across all conditions. For OCS and SPS very similar time courses were obtained from the MFT solutions extracted from the average MEG signal. Figure 3 shows that for REMS, pontine current density, direction of flow and spatial distribution within the brain stem were broadly similar to those of the waking state saccades. The REMS PN activations for the two subjects with only nine REMS to the left each were more noisy than for the subject with 16 REMS, but the same pattern of current reversal was clearly evident around saccade onset (time 0) as for OCS and SPS. We conclude that for movement to the left the direction of current flow on either side of the brainstem and details of the rapid change around eye movement onset were very similar for all conditions and subjects.

Figure 4 shows the location of PN ROIs obtained from the analysis of the average signal and examples of their corresponding activation curves (for the Talairach coordinates see Table 2). For horizontal eye movements the current direction was reversed on the other side of the pontine midline, as would be expected if the two halves of the PN were organizing agonist and antagonist motor neurons serving the same movement. This is clearly evident in the examples in Figure 3 (all subjects and conditions) and Figure 4 (one subject SPS condition). For saccades to the right the current flow was the reverse of the left-sided pattern. For up and down OCS and SPS, when the activity was bilaterally similar in the mesencephalic gaze centers, the current change was the same for both sides of the pons. The saccade-to-saccade interval of ~4 s produced a comfortable rate of eye movement, which was reflected in the rhythm displayed by the activation time course (Fig. 4*D*). No interval of effectively silent PN activity between saccades was present, possibly because gaze center activity was required, at least in part, to maintain fixation. The general features of PN activations for eye movement in different directions demonstrated in the displays of Figures 3 and 4 were identified in the averages for each subject in all conditions (OCS, SPS and REMS), provided enough single trials were available (typically nine or more).

In summary, the examination of the PN activations from the average and single trial data showed intermittent activity for many hundreds of milliseconds both before and after saccade

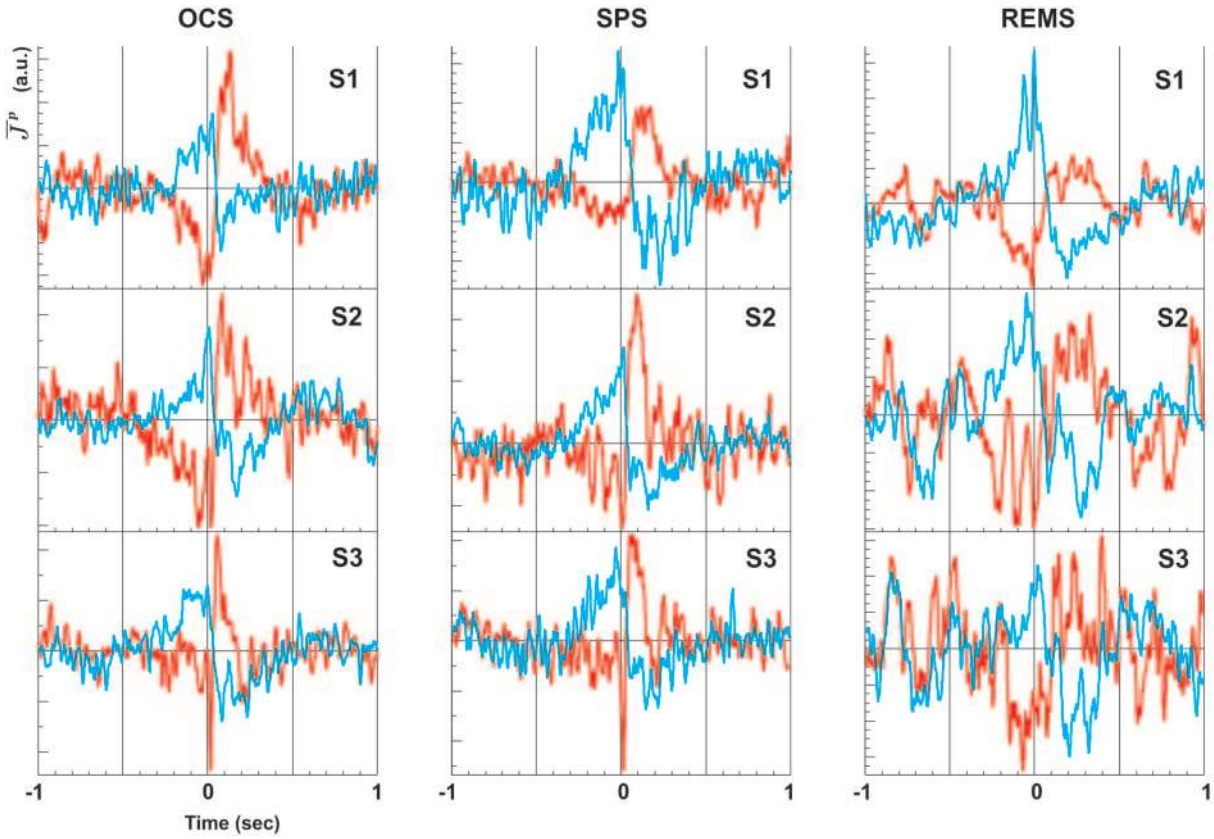


**Figure 3.** The time course of average activations in the left (blue curves) and right (red curves) PN for saccades to the left for OCS, SPS and REMS for each subject. *X*-axis values are 1 s before to 1 s after eye movement, which was at 0. The quantity, $\bar{J}^p$, on the *Y*-axis is the ROI-wide average of the component of the current density vector along its dominant direction at the peak (arbitrary units).

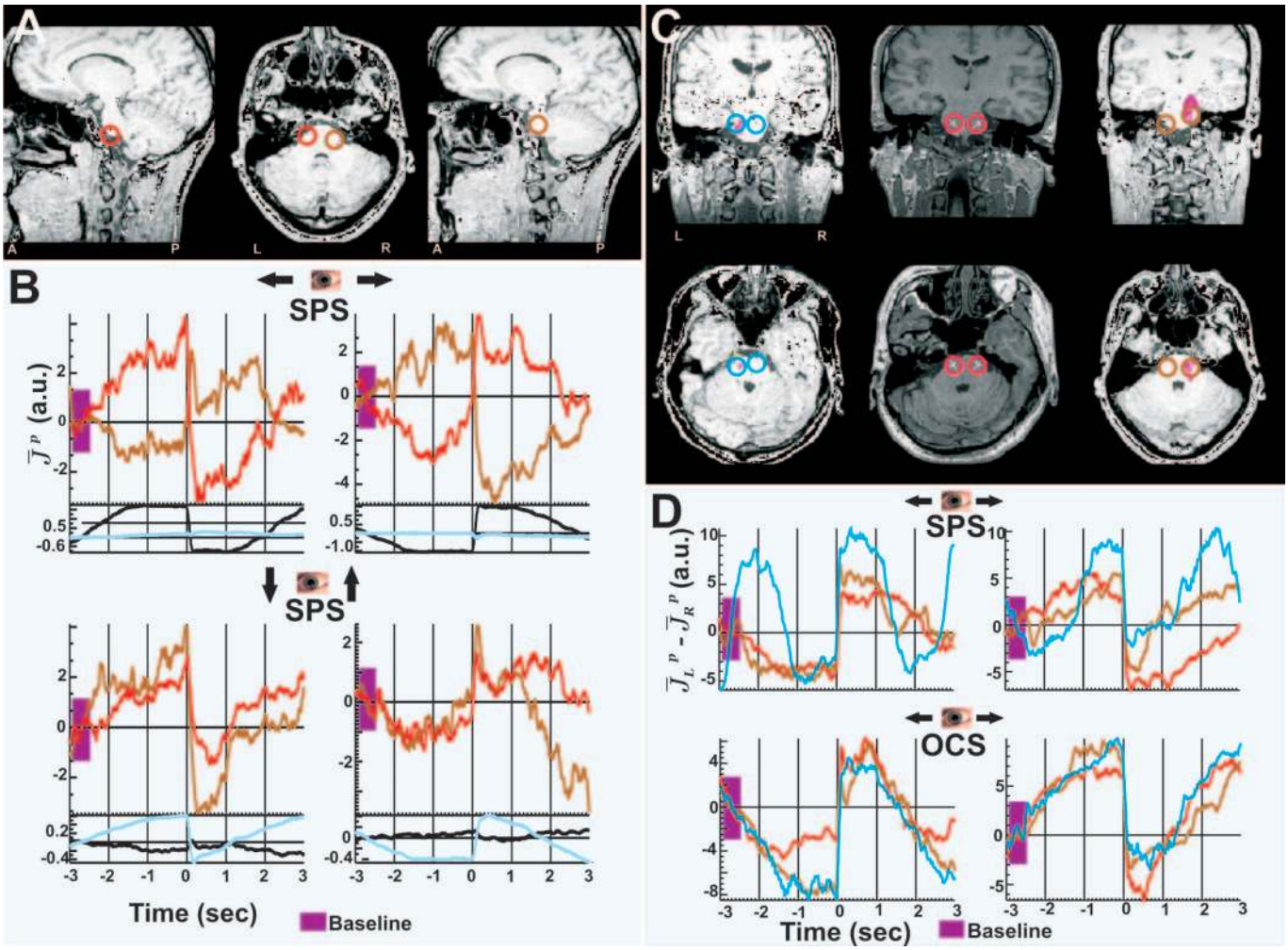


**Figure 4.** MFT estimates for the current density in the pons for OCS and SPS extracted from the 6 s long, low-pass filtered below 20 Hz MEG signal. (*A*) Red and brown circles mark the left and right ROIs for PNs for subject S2 (see coordinates in Table 2). Each ROI is superimposed on the left and right sagittal MRI slices and both are displayed together on a transaxial slice (middle). (*B*) MFT estimates for $\bar{J}^p$ (defined as in Fig. 2), for the left (red, $\bar{J}^p_L$) and right (brown, $\bar{J}^p_R$) PN ROIs extracted from the average MEG signal and subsequently smoothed with running average filter of 0.1 s. The results are for subject S2 for SPS directed towards left, right, up and down, as verified by the corresponding EOG traces (horizontal–black, vertical–blue). (*C*) The pontine ROIs of three subjects in coronal (upper) and transaxial (lower) MRI slices. (*D*) Subtraction (enhances the difference) of MFT solutions in right PN from those in left PN ($\bar{J}^p_L - \bar{J}^p_R$), during SPS and OCS, eye movement in horizontal directions in the three subjects (traces of each subject bear the color of their pontine area in *C*).

onset. The slow components captured in the 6 s long data showed that the activity across trials merged, yielding a steady almost rhythmic activity for OCS and SPS. As expected, variability was higher away from the saccade onset. The patterns of activations agreed with the predictions for current flow changes in the brain stem for both horizontal and vertical movements, and they were particularly clear for the OCS case where the auditory cue provided a precise time locking signal. Horizontal movements showed increased current flow in the PN ipsilateral to the movement while vertical movements showed the activity bilaterally. Horizontal and vertical gaze centers were too close to resolve, so the activations from the left and right PN ROIs sampled activity from them both. The same pattern of pontine activity was seen for SPS across all subjects.

### *Measurement of SNR from Cortical and Brainstem Structures*

In Figure 5 the SNR results for S3 are displayed for left OCS (Fig. 5*A*), right OCS (Fig. 5*B*) and leftwards REMS (Fig. 5*C*). Subject S3 had the lowest SNR values for REMS. In each case the display shows the SNR curves for the right and left pontine nuclei frontal eye fields and visual cortices. No evidence was found for shadowing of SNR patterns from one area to another. Specifically, there was no evidence for high SNR values in the brainstem activations when the cortical generators had high SNR, even for the relatively low SNR REMS activations. Before OCS onset to the left and right the SNR curve for the ipsilateral PN is low except for a fairly well defined peak in the last 100 ms before saccade onset. This has a rather modest value of 3 for OCS L and 6 for OCS R. For OCS to the left after saccade onset the left (ipsilateral) PN produces activations with a high SNR (28). For both OCS L and OCS R the contralateral PN produces the higher SNR in the 200 ms before saccade onset and again ~200 ms after saccade onset (with SNR peaks well above 20). In REMS to the left the ipsilateral and contralateral PN activations produce similar SNR values with peaks around 4. The FEFs for all three conditions show low SNR before and after eye movement because of poor time locking. The SNR displays for the

**Table 2**
Talairach coordinates of ROIs

| Row | Subjects | | Pons | FEF |
|---|---|---|---|---|
| 1 | S1 | L | –8 –23 –33 | –42 15 44 |
| | | R | 10 –22 –32 | 40 10 42 |
| 2 | S2 | L | –11 –25 –41 | –48 3 37 |
| | | R | 12 –25 –31 | 36 –3 33 |
| 3 | S3 | L | –11 –24 –24 | –34 19 21 |
| | | R | 5 –21 –25 | 31 24 28 |
| ROI | SMA | | Precuneus | Parietal |
| 4 | L –5 –17 67 | | 0 –49 39 | L –56 –40 31 |
| | R 2 –18 68 | | | R 52 –36 31 |
| ROI | R Amygdala | | R PHG | R Pons |
| 5 | 19 –3 –24 | | 23 –18 –23 | 11 –21 –20 |

Rows 1–3, Talairach coordinates (mm) for the pontine ROIs shown in Figure 4*C* and FEF ROIs used in Figure 4. Talairach coordinates for common activity across the three subjects as identified by SPMs ($P < 0.005$), Figure 4*A*, row 4, Figure 4*B*, row 5.

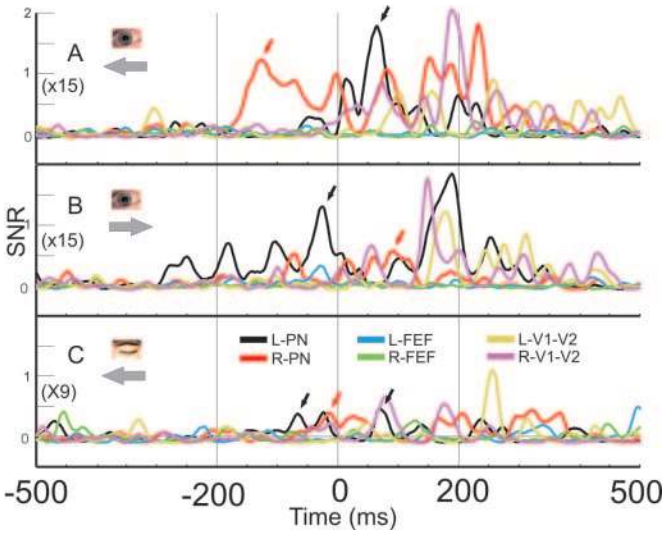


**Figure 5.** (*A*) The SNR of six ROIs for horizontal OCS and REMS to the left for subject S3 for the range –500 ms to +500 ms relative to the saccade onset. For each ROI the SNR value for each latency, *t*, is computed from the single trial MFT solutions in a 21 ms window centered at *t*. Red and black left and right pontine nuclei, blue and green left and right frontal eye fields, olive and purple left and right V1 and V2. The SNR value per trial is shown by the scale on the *Y*-axis. The SNR for the set is obtained by multiplying by the number of trials, i.e. 15 for the case of OCS to the left. The black and red arrows show the major peak of the pontine SNR before and after the saccade onset. (*B*) SNR for OCS to the right (number of trials = 15). (*C*) SNR for REMs to the left (number of trials = 9).

visual cortex show high values in both REMS and the awake conditions some time after eye movement onset, with particularly high SNR values (25–30) ~200 ms in the awake conditions.

### *Cortical and Limbic Activations*

The instantaneous MFT solutions showed activity over wide cortical and subcortical areas in all conditions OCS, SPS, REMS, REMB and ECW. The SPM maps identified saccade related changes in activity between active and control conditions, arranged in time according to the latency interval separating the center of the active latency window from the saccade onset. In the discussion of these maps we emphasized saccades to the left because only in this condition did we had have enough trials in REMS to allow us comparison across all three conditions. The Talairach coordinates of the regions consistently identified across subjects are given in the lower part of Table 2.

The SPM comparisons between REMS and the other conditions identified persistent, statistically significant changes in each subject, showing increased activity in the supplementary motor area (SMA), in the orbitofrontal cortex (OFC) and amygdala, and decreased activity over precuneus and the bilateral inferior parietal areas. To determine which cortical activations were due to the REM state or specifically to REMS, SPMs with 100 and 500 ms windows were used to contrast REMS with OCS, ECW and REMB. The SPMs for the REMS versus ECW using a 100 ms window are shown in Figure 6*A*. The increase in SMA and the reduction of activity over precuneus and bilateral inferior parietal areas persisted in the REMB versus ECW comparison. No statistically significant changes in activity were identified in SMA, precuneus and parietal areas for the REMS versus REMB comparison. It was therefore concluded that the increase of SMA activity and decrease in precuneus and parietal activity are state properties of REM.

Grand-SPMs with long (500 ms) windows also showed REMS-related increase in activity in the OFC and amygdala in both REMS versus ECW and REMS versus REMB contrasts, for a few hundred of milliseconds on either side of the REMS onset. These activations were bilateral in REMS versus REMB comparison, but more prominent in the left OFC and right amygdala for REMS versus ECW. Grand-SPM comparisons with the smaller latency windows (12 ms) provided evidence for a right hemisphere sequence of activations prominent for REMS in the 100 ms before REMS onset, leading from OFC to the amygdala, parahippocampal gyrus (PHG) and finally the brainstem, as shown in Figure 6*B–D* for the REMS versus ECW comparison. Well after the REMS, first the left OFC and amygdala (180–215 ms) and then only the right amygdala (240–265 ms) were consistently reactivated in all three subjects.

### *Grand Average SNR Across Conditions for Cortex and Brain Stem*

For some areas, e.g. the FEFs, MFT solutions for individual trials showed activity before eye movement with wide variations in timing so that the averaged single trial signals showed little significant activity and no significant SPMs were found. To examine whether both well-time-locked and labile activity were present, we computed for each subject the SNR curve, for each condition and eye movement direction. The SNR curves were then averaged across subjects and SPS and OCS conditions for each eye movement direction. A similar computation was made for the ECW condition matching as well as possible the number of trials used in the computation of each SNR curve (see Table 1). The resulting grand averaged SNR curves for eye movement to the left and right are shown for the PN, V1–V2 and FEF in Figure 7. In agreement with the results for the single subject in Figure 5, the SNR curve for the PN is higher on the contralateral side before eye movement and on the ipsilateral side after movement. The SNR is again high for the visual cortex (V1–V2) which is sustained for a few hundred milliseconds after saccade onset. The highest SNR values for FEF activity is 30–70 ms before the eye movement so there is a well-time-locked bilateral FEF activity that directly precedes the eye movement.

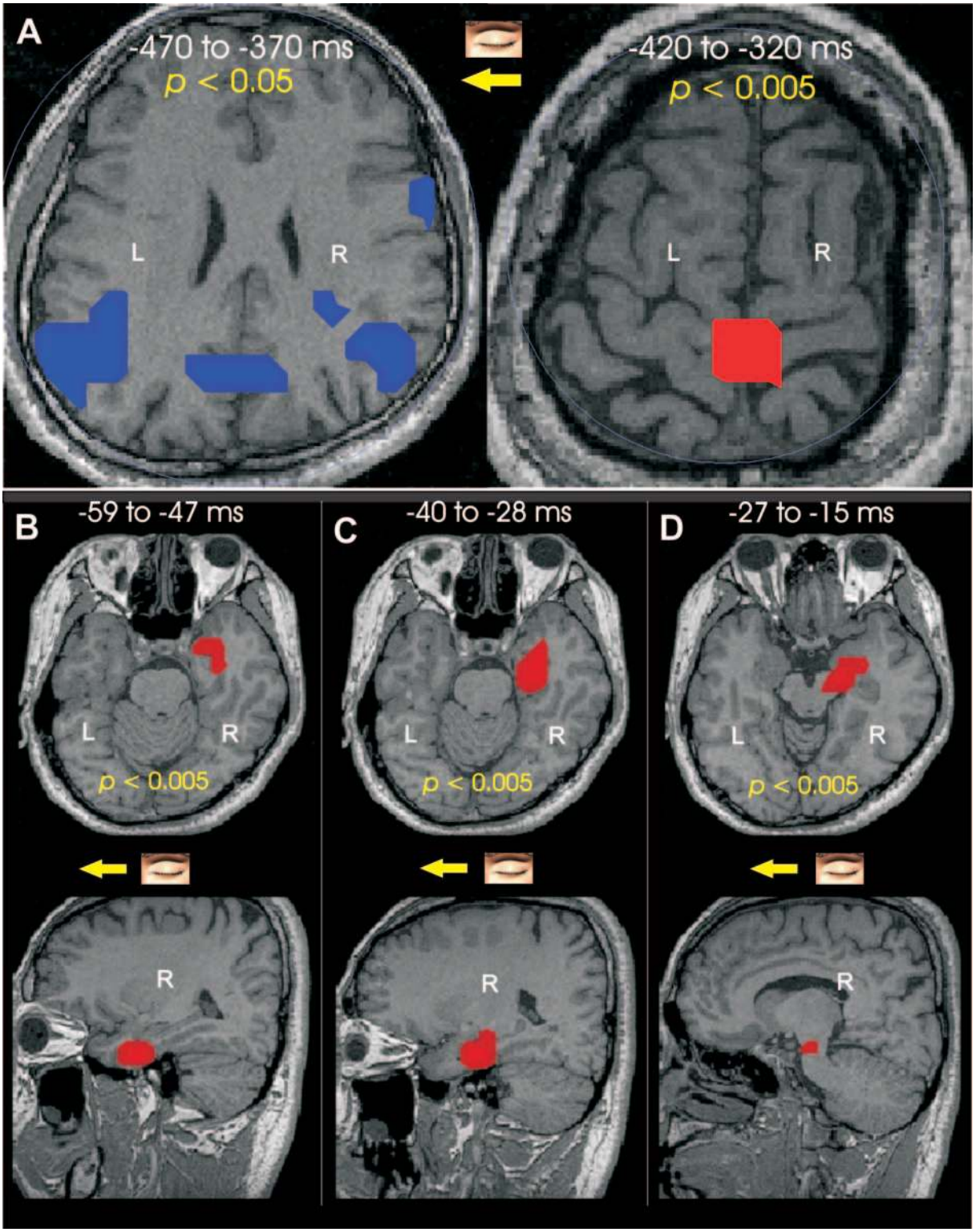


**Figure 6.** Grand SPMs for leftward eye movements. The loci of common changes are identified after the data from each subject are transformed into the Talairach space (coordinates of areas in Table 1). The common loci for the three subjects are displayed after back-transforming the results and projecting them onto the MRI of one subject (red — increase, blue — decrease; the time interval and the threshold *P*-value are printed inside each figurine). (*A*) Examples of the persistent changes from comparison with long (100 ms) windows, left picture REMS contrast with ECW, right picture REMS contrast with OCS and SPS. (*B–D*) Axial and sagittal MRI slices for three successive SPMs leading to saccade onset (the contrast is REMS to the left versus ECW using 12 ms windows). The SPMs show a sequence of relative increase of right hemisphere activity in REMS beginning in the orbitofrontal cortex and amygdala (*B*), followed by activity in the PHG (*C*) and finally PN (*D*).

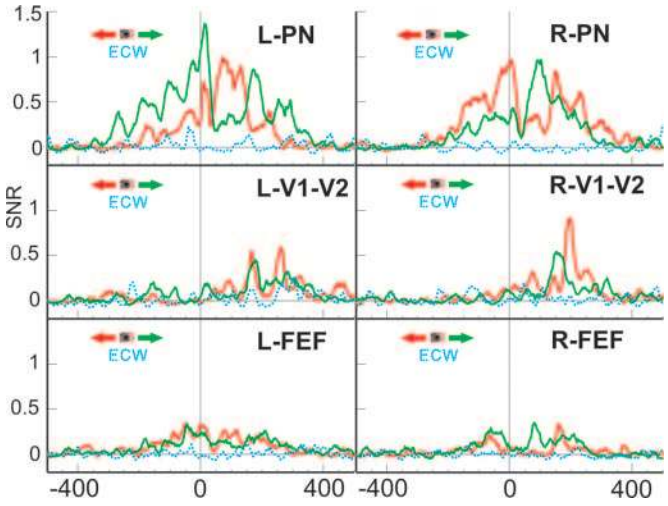


**Figure 7.** The grand averaged SNR for OCS and SPS to either the left (red curves) or the right (green curves). The SNR for each subject is computed for the same areas and with the same parameters as for the SNR computation for S3 in Figure 5. The results are then averaged across the three subjects. In addition the grand averaged SNR for the ECW condition was computed using the same number of trials as OCS and SPS, if available (dotted blue curve). The left and right columns are for the structures on the left and right side of the head. The SNR values shown reflect the quality of the signal at a single-trial level. To obtain an SNR estimate of the corresponding grand-averaged signal, the *Y*-axis should be scaled by (grand average of the number of trials across subjects and the two conditions) 13.6 for the left movements (red curves) and 11.3 for the right ones (green curves).

### *Timing and Interaction of Activated Brain Areas*

Grand post-MI results will be reported to reveal the pair-wise relationships between the areas already identified from our SPM analysis, e.g. FEF, OFC, auditory and visual cortex, amygdala, PHG with the PN and/or the EOG. REMS will be described first as those results are the most complex. The top half of Figure 8*A* shows pair-wise comparison for left REMS between four areas — left PN (blue), right PN (green), left FEF (red) and right FEF (orange) — and the EOG. The marked islands of the map correspond to the pairwise comparisons that exceed the 35% threshold for the normalized MI for each subject. The *X*-axis gives the timing of the ROI activity with negative values before eye movement and positive times after. The *Y*-axis shows the delay of the EOG, so that positive (negative) values correspond to ROI activity before (after) the EOG. The dotted iso-ocular line through the origin corresponds to linkages leading to EOG activity at the onset of eye movement. Hence, the large blue island at $X$ = –300 ms, $Y$ = 250 ms straddles the –50 ms line and the iso-ocular line extending almost to the +50 ms line; it shows activity of the left PN 300 ms before eye movement which effects the EOG from 50 ms before to 50 ms after eye movement.

The broad structure of the MI islands in Figure 8*A* shows vertical bands that correspond to persistent activity in PN (blue and green colors) preceding and following EOG activity (e.g. positive and negative delays) but not always leading to eye movement (far away from the iso-ocular lines through or close to the origin). Strong FEF (red color) activity follows on from activity in the EOG ($Y < 0$) at about –500 ms ($X \sim -500$) before REMS onset. Nearer to the time of movement (zoomed area and above the $Y$ = zero line), activity in both right and left PN in the 50 ms before movement is linked to EOG activity after the movement. Below the zero line again the PN is active bilaterally with right FEF activity following the EOG activity. The MI map for REMS is dominated by MI islands spread in fairly regular latency bands well away from the iso-ocular line with $T_{EOG} \sim 0$. Three hundred milliseconds before the beginning of REMS, there is sharp (50 ms long) activation in the ipsilateral PN (blue contours in Fig. 8*A* top left), which is linked by an iso-ocular line to the EOG all the way to the beginning of movement. At about the same time activity is evident in the contralateral PN, but this one is linked to EOG activity 250 ms before REMS, $T_{EOG} < -250$ to – 200 ms, possibly an aborted REMS. The large-scale pattern of the MI map suggests a periodic modulation at ~4 Hz consisting of successive attempts to initiate REMS, which occasionally succeed.

The MI was computed for left saccades between the FEF and the pontine nuclei with the EOG, with the overlap for all subjects and more than one condition. Figure 8*B* shows the common activations obtained with the threshold set at 20%. When all conditions were combined, high MI with the EOG was identified for the left and right pontine nuclei only after saccade onset (all activity seen in the zoomed areas is right of (after) the iso-ocular line with $T_{EOG} = 0$). For REMS and OCS common FEF activity was evident well before and after the saccade. Specifically, contralateral FEF activity, 300–200 ms before the onset of the saccade, links with the EOG activity immediately after saccade onset. Contralateral FEF is seen also during the 80 ms before saccade onset to link with the EOG 50–100 ms after saccade onset.

Figure 9 shows the contours marking islands of high MI values that are common across the three subjects, for OCS to the left and right. This is a much simpler picture as with a threshold of 30% all the activity fell close to the iso-ocular line. In view of this the figures of the left and right eye movement (blue and green background) were combined to show the islands of high MI near the iso-ocular lines. The zoomed areas of activity are to help identification of the ROIs. Again the *X*-axis is the ROI latency and the *Y*-axis the EOG delay. Linked activity between the PN, FEFs with the EOG, is shown in the top half of the figure (Fig. 9*A*), and between the auditory and visual cortices with the EOG in the bottom half of the figure (Fig. 9*B*).

For eye movement to the left Figure 9*A* shows activation in both FEFs before movement. The ipsilateral FEF some 270 ms, and the contralateral ~200 ms and again at between 80 and 30 ms before the saccade occurred. Both these activations are linked to the EOG after the start of movement ($T_{EOG} > 0$). The contralateral PN activation at ~100 ms before saccade onset was linked to the EOG activity again just after the start of the saccade. For rightward movements the contralateral FEF was active at 230 ms and again at 60 ms before movement, again related to the EOG after saccade onset. The contralateral PN activity just before saccade onset was also linked to the EOG activity, but again just after the start of the saccade. For both left and right directions the MI map shows that EOG signal after eye movement onset is linked to FEF and pontine activations intermittently for the next 300 ms.

Figure 9*B* shows results for the auditory and visual cortices. The most salient linked activity was seen during the 200 ms preceding and following horizontal eye movements. SPS MI is not illustrated here but it follows for each subject the same general trend as for OCS, however voluntary initiation makes timing less precise across subjects. In summary, the linked acti-

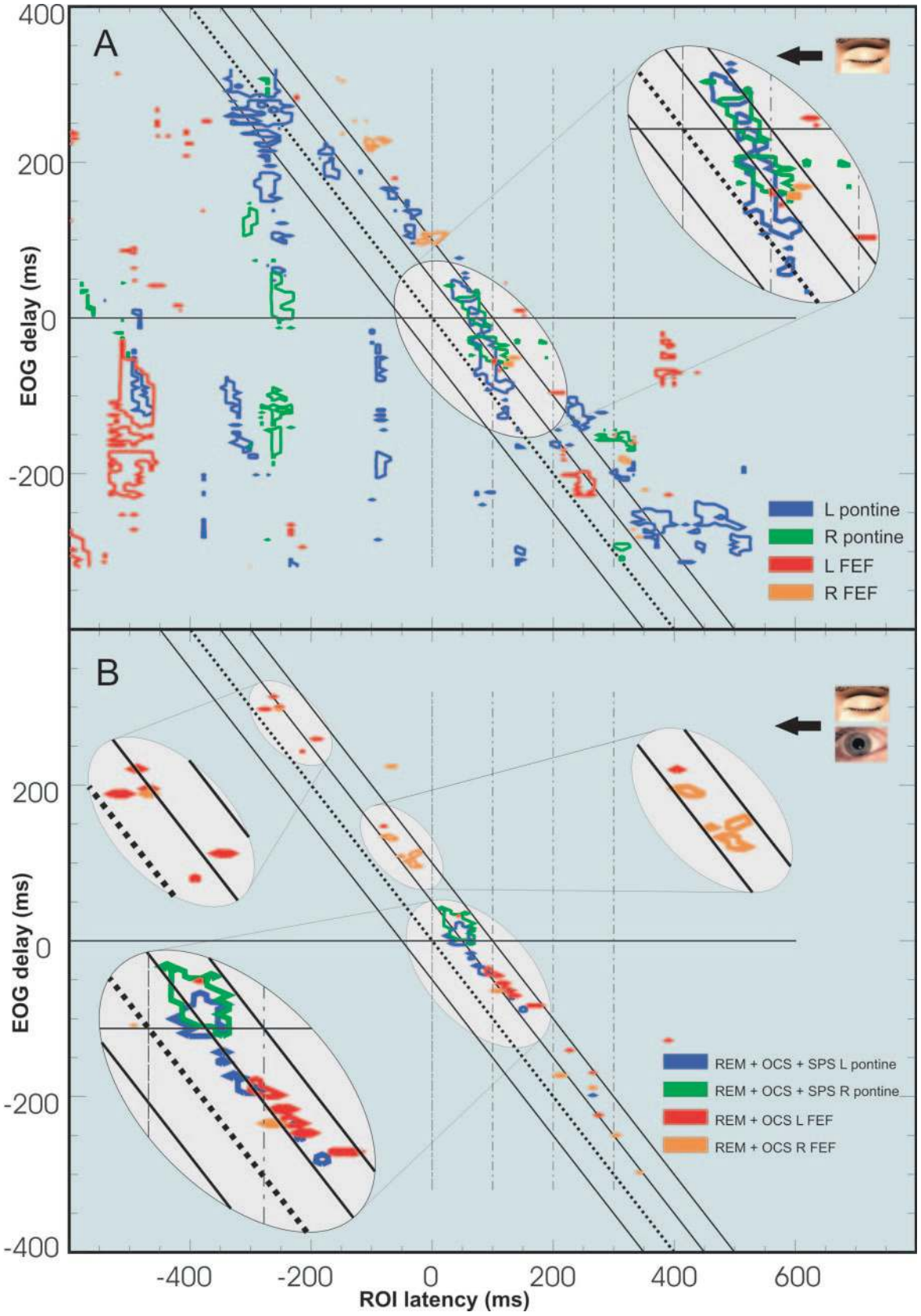


**Figure 8.** Mutual information analysis for eye movements to the left for REM and combined across conditions. Each diagram includes four iso-ocular lines 50 ms apart, with the TEOG = 0 shown dotted. Portions of the diagram where MI islands cluster are expanded to aid visual inspection. (*A*) The MI is computed between left and right pontine and left and right FEF ROI activations and the EOG signal for REM-L. The contours mark high common MI values (above 35% of max value for each subject) (*B*) Islands with common high MI values (above 20% of max value for each subject) for saccades to the left and more than one conditions for the same ROI–EOG pairs as (*A*).

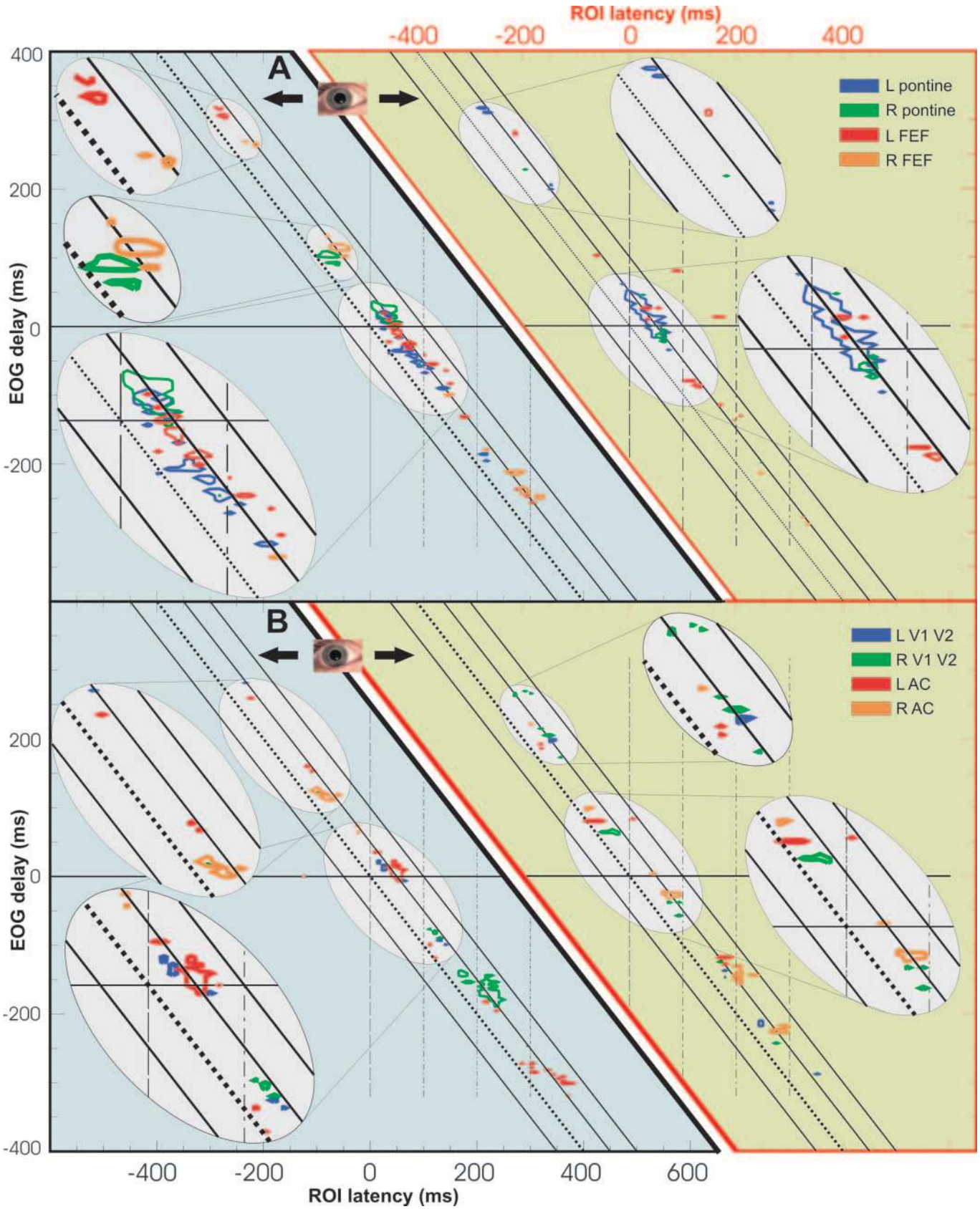


**Figure 9.** Mutual information analysis from three subjects for the OCS. Each diagram includes four iso-ocular lines 50 ms apart, with the $T_{EOG} = 0$ shown dotted. Portions of the diagram where MI islands cluster are expanded to aid visual inspection. The contours delineate islands with high MI common for all subjects (above 30% of max value for each subject). The color of the contour codes for the ROI–EOG high MI islands. Left panels, movements to the left (blue background); right panels, movement to the right (green background). (*A*) The MI is computed between left and right PN and left and right FEF ROI activations and the EOG signal. (*B*) The MI is computed between left and right auditory cortex (AC) and left and right visual cortices (V1/V2) and the EOG signal.

vations in Figure 9 are clustered to the right of the iso-ocular line with $T_{EOG}$ = 0 demonstrating a direct relationship between the EOG signal after saccade onset and neuronal activity in the FEFs and brain stem well before and after the saccade.

### *The Network Leading to Saccades*

Figure 10 shows the influence diagram summarizing the essence of the information contained in many grand-MI maps (linkages between ROIs and EOG common to all subjects in

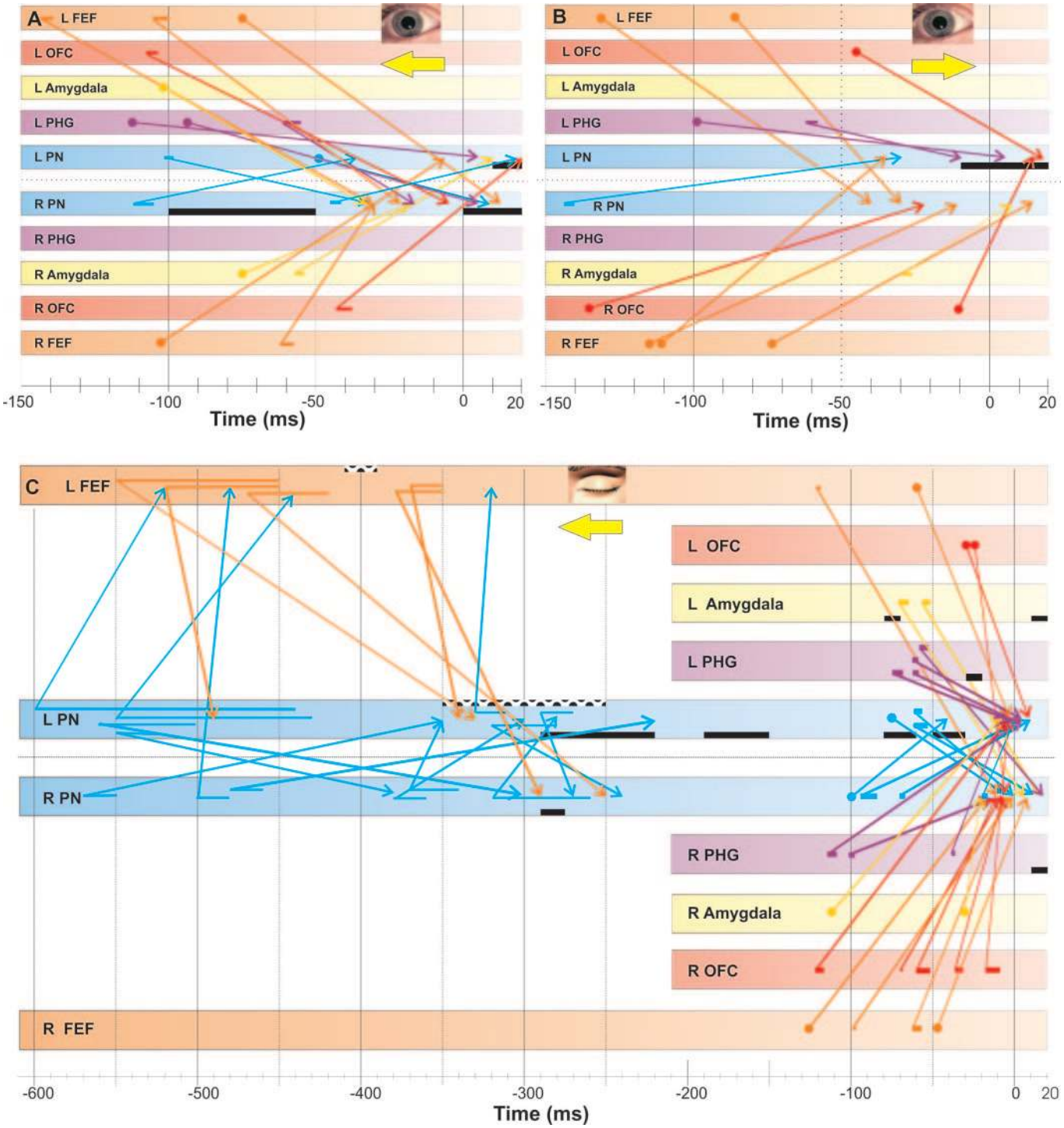


**Figure 10.** Arrow maps for linkages between regional brain activations common to all subjects (normalized common MI threshold set at 30%) leading to eye movements. (*A*) OCS to left. The colored bands show L FEF, L OFC, L amygdala, L PHG and L PN, the five areas on the left. The next five areas below are in the reverse order but on the right side. Arrows show all MI linkages related to PN activity around saccade (–50 to +20 ms). The black heavy striped blocks at the top of ROI bands represent MI links between ROI and EOG activity just before the saccades, the heavy filled black blocks at the bottom of the bands represent ROI and EOG activity immediately after the saccades. The link to EOG is seen for both L and R PN (linked to post eye movement EOG) and it is more prominent for the R PN. (*B*) OCS to right. The layout is as in *A*. The link between ROI and EOG is only seen for L PN and again only for post eye movement EOG. (*C*) L REMS. Areas are in same order as in (*A*). For PN and FEF the display is extended to –600 ms. The blocks at the top and bottom of bands show again links with EOG. Links to EOG before REMS are identified in the L FEF (around –400 ms) and in the L PN from –350 to –250 ms.

Figures 8 and 9 and the many more MI maps for ROI to ROI linkages). We show the results for the OCS saccades to the left (Fig. 10*A*) and right (Fig. 10*B*), and for the REMS to the left (Fig. 10*C*).

For both OCS to left and right both FEFs link with the PN, with the strongest links to the right PN. Less frequent contributions are also identified from the OFC, amygdala and PHG to the PNs. The EOG-based MIs show that most activations preceding saccades are to the contralateral PN. Almost all the MI linkage in the figure corresponds to MI links leading to EOG and PN activity after saccade onset, and are therefore related to maintenance and stopping of eye movements. In OCS the pacing by the tone limits the time available for eye movement preparation, imposing a fast sharp onset on the saccade, and thus limiting the usefulness of direct comparison of the influence diagrams for OCS and REMS in the same timescale.

Figure 10*C* shows the interactions in REMS to the left between the same areas. The time period shown is extended to 600 ms before REMS for the linkages between FEFs and PN. Intermittent and possibly rhythmic interactions are seen for many hundreds of milliseconds. The diagram shows how the early interactions between left FEF and PN lead to the PN–EOG linkage. Links with long delays between very early L FEF and R PN activity converge with short delay L FEF activity on the L PN ~350 ms before REMS. The heavy striped block on the upper part of the L FEF and L PN bands provide the best direct signature for saccade initiation, linking respectively activity around –400 ms for L FEF and from –350 to –230 ms in L PN to EOG before REMS onset. The interactions in the 150 ms prior to eye movement intensify to include bilateral activity in the FEF, OFCs amygdala and PHG with the right hemisphere more active than the left.

## Discussion

This study shows that eye movements are the outcome of the integration of activity in several major brain areas over hundreds of milliseconds. A complex but well organized sequence of events is associated with the preparation, execution, control, and stopping of eye movements, for each saccade condition and direction. The sequence is particularly long lasting for REMS. The time ordering of interactions was identified from the significant linkages in activations between the FEF and the PN but also between the OFC, amygdala, PHG and the visual cortex which were also shown to be correlated with the eye movement.

### *Imaging Brain Stem Activity*

When we embarked on this study there was no direct evidence for brainstem tomographic imaging with MEG, but earlier studies provided ground for some optimism about its feasibility. Electrical measurements of brainstem potentials have been demonstrated for auditory evoked responses (Moller *et al.*, 1982) and median nerve stimulation (Aage *et al.*, 1986). Magnetic measurements in pigs confirmed the presence of MEG signal generated by current changes in the brain stem (Hashimoto *et al.*, 1996) and was followed by reports of human cerebellum activity recorded outside the skull with MEG (Tesche and Karhu, 1997). The MFT solutions reported in the present study demonstrate that activity in the pontine gaze centers can be imaged millisecond by millisecond (Fig. 2). The topography of the sharp changes in current flow close to eye movement was exactly as would be expected if each PN ROI sampled activity from both horizontal and vertical gaze centers. As shown by the activation curves, left and right PN current flow reversed for opposite directions of the saccade and in each case the pattern was mirrored around the time of the saccade onset. The PN activations had the same sign across the midline for up and down saccades. The average PN activations showed these patterns for all three subjects and in all conditions where enough single trials were available. Single trial MFT solutions identified robust brainstem activations with high SNR; there was no evidence of cortical reflections. The lower SNR for REMS was still respectable, even for the worst subject (Fig. 5). Taken together these results demonstrate the feasibility of accurate imaging of brainstem centers in both the awake state and during sleep. They therefore extend to the level of the brainstem the claim for accurate localization using post-MFT analysis of non-invasive MEG signals demonstrated recently at the level of the primary visual cortex in a combined MEG and fMRI study (Moradi *et al.*, 2003).

### *Activations Related to Eye Movement When Awake*

Around saccade onset MFT identified activity in brainstem and cortical areas including both ipsilateral and contralateral FEFs, as has been shown by PET and fMRI studies in man (O'Sullivan *et al.*, 1995; Petit *et al.*, 1996; Luna *et al.*, 1998) and from cellular recordings in primates (Schall, 1991; Segraves and Park, 1993; Leigh and Zee, 1999). In the awake saccades pontine activity was shown to control the stopping of the movement by activity in the 100 ms preceding saccade onset (MI from Fig. 9) and continuing for some 50 ms after. During the stopping of eye movement a ramping down of the average current flow was evident in the PN.

At the cortical level activity is present for hundreds of milliseconds around saccade onset in both ipsilateral and contralateral FEFs and is linked to PN and EOG activity at or just after eye movement. The FEF activation is ~100 ms before activation of the contralateral PN, some 40–50 ms before the movement. For the same eye movement direction, high MI was identified common to all subjects and conditions (including REMS), suggesting some common core programming of the saccade in the three conditions. Saccadic eye movements as shown by cellular recordings in primates are ballistic in nature, with the direction, amplitude and velocity programmed before initiation of the movement (Leigh and Zee, 1999). It is thus likely that the multiple bilateral FEF activations seen in Figure 10*A*,*B* are related to the initial ballistic signal. Furthermore neural selection and control of visually guided movements are steered by stochastic growth of movement related activity (Schall and Thomson, 1999), very much like the ramping up seen in our cortical and pontine activations. Evidence was recently provided for FEF coding both readiness and intention for saccade generation (Connolly *et al.*, 2003) in agreement with the growth of FEF activity seen in Figure 7*C*. The relationship of FEF and PN activity was different among the conditions, but in general the laterality of PN activations was well defined around saccade onset while the FEF activations were seen bilaterally. The dorsolateral prefrontal cortex in the monkey is also related to saccadic eye movements for both the long-term pre-and post-saccadic periods (Funahashi *et al.*, 1991). We found OFC activity to be directly related to PN activation ~100 ms before eye movement. There was also bilateral amygdala involvement in movements to the left but not to the right, and left para-

hippocampal gyrus activity on both left and right movements. This amygdala asymmetry was unexpected. There is however considerable literature on eye movement desensitization reprocessing therapy given for post-traumatic stress disorder. It is thought that amygdala and hippocampal gyrus activation during eye movements facilitate the reprocessing of traumatic memories (Stickgold, 2002). Our studies certainly show activation in these structures and on the basis of the amygdala asymmetry they suggest that center to left eye movements may be more effective than center to right.

Both SNR analysis (Figs 5 and 7) and the MI analysis (Fig. 9*B*) showed post-saccade activation of the visual and auditory cortex. The linkage between EOG transients 50 ms after saccade onset to activity in visual cortex 150 ms later (Fig. 9*B*) is consistent with suppression of visual processing around saccade onset and resumption 200 ms later (Burr *et al.*, 1997).

### *Eye Movements in Sleep*

REM sleep eye movements showed activation of the same structures, FEFs and PNs, as did the waking saccades, however over long timescales the timing and sequences of activation were different. Cortical and brainstem activity, in the 250–350 ms leading up to REMS, showed that the initiation of eye movement is surprisingly longer than the 200 ms reported for animals (Cespuglio *et al.*, 1975; Nelson *et al.*, 1983; Paré *et al.*, 1990). The dominant PN activity is intermittent, organized in bursts at ~4 Hz. Throughout this time there is a dialogue between PN and FEF with reciprocal activations but with the PN activity being always more prominent. This suggests that during REM the PNs drive the eye movement and the FEF receives feedback of this activation. The dominance of the pontine generators, at the expense of the cortex, is consistent with the theory that endogenous PN activity leads saccade generation in a bottom-up flow of information (Calvo and Fernandez-Guardiola, 1984).

There is no direct evidence of PGO waves for humans. Nevertheless, the periodic PN activation shown in this study is similar to the occurrence of PN activity and PGOs in cats, which are thought to have a common generator, the caudoventral pontine tegmentum (Vanni-Mercier and Debilly, 1998). In cats PGO waves can be unilateral or bilateral events, single or in bursts of doublets, triplets or even more (Cespuglio *et al.*, 1975; Datta and Hobson, 1994) with intraburst intervals of 48–259 ms (Vanni-Mercier and Debilly, 1998). Importantly not every PGO wave is followed by an eye movement. These results suggest that for REMS a build-up of excitability is needed before a threshold is reached for triggering an eye movement. This build up has been shown in the waking monkey for FEF (Hanes *et al.*, 1995) and supplementary FEF (Schlag-Rey *et al.*, 1997) neurons. We suggested that the periodic activity seen in the PN in this study is part of a phasic process in humans leading to REMS.

### *Cortical Activations in REM*

PET studies of REM sleep have found activation in a large number of structures, including FEF, dorsolateral prefrontal cortex (DLPFC), the midline attentional system and the parietal visual spatial attentional system (Hong *et al.*, 1995; Maquet *et al.*, 1996; Nofzinger *et al.*, 1997; Braun *et al.*, 1998; Peigneux *et al.*, 2001). Our data also show that other cortical systems, R and L, OFC, Amygdala, PHG and FEF are involved with the generation of REMS via their influence on the PN (Fig. 10*C*). The slow temporal resolution of PET and the different baselines used in the different studies makes a detailed comparison between PET studies and our own difficult. Interestingly Hong *et al.* found that the FEF (and DLPFC) were only significant for the right hemisphere, adding support to our finding that left-sided REMS were most common. We found increase in SMA activity both for long periods in REMB and at ~200 ms before REMS, which to our knowledge has not been reported in any PET study. Awakenings during the night with abnormal motor activity is now well recognized. Some of these abnormal nocturnal motor episodes are due to SMA seizures (Tachibana, 1996). The finding of SMA activation in our study suggests a possible link between 'awakening epilepsy' motor abnormality and SMA pathology (Niedermeyer, 1991).

### *Limbic Activations in REM*

Some studies using PET in man (Maquet *et al.*, 1996; Nofzinger *et al.*, 1997; Braun *et al.*, 1998) have shown widespread activation of limbic structures during REM sleep. However it is not possible with PET to distinguish between tonic activation due to the REM state and a phasic one related to REMS. The results from this study show both a background activation of limbic areas linked to the REM state and also directly linked to PN activation, leading to REMS. The grand SPMs for REMS showed a highly statistically significant amygdalo-PHG-PN sequence prominent from the right hemisphere in the last 100 ms before REMS. This sequence is likely to contribute to the build-up of excitability in PN rather than be directly involved with REMS initiation because it did not appear strongly in the MI analysis. The sequence provides a link between studies in cats (Jacobs and McGinty, 1971; Calvo and Fernandez-Guardiola, 1984; Sastre *et al.*, 2000), monkeys (Benca *et al.*, 2000) and rats (Deboer *et al.*, 1998) with earlier human studies of direct amygdala stimulation (Halgren *et al.*, 1978), and recent imaging studies (Maquet *et al.*, 1996; Nofzinger *et al.*, 1997; Braun *et al.*, 1998). Limbic activation during REM is thought to be related to several clinical conditions such as emotional arousal and threatening dream content (Peterson *et al.*, 2002), post-traumatic stress disorder (Stickgold, 2002) and mood disorders, especially depression, which is accompanied by an increase in REMS (Gillin and Borbély, 1985; Schenck *et al.*, 1992). As a target for future studies we put forward the speculation that the amygdala and PHG activations could reflect, respectively, biases toward emotional processing (Fernandez *et al.*, 1999) and learning (Stickgold *et al.*, 2001) during REM, and possibly play a role in the emotional arousal of the parasomnias, nightmares and REM sleep behavioral disorders.

In summary, we have MFT analysis of MEG signals provided real-time tomographic information and precise timing relationships between major areas involved in the generation of eye movements, specifically the brainstem gaze centers and cortical activity. The MEG methods we have described make possible human investigations that previously could only be carried out in animals, they are thus potentially relevant to studies of the physiology and pathology of these highly important and rather inaccessible regions.

## Notes

We wish to thank our subjects for their participation in this study and all staff of the laboratory for Human Brain Dynamics for their contribution during sleep recordings and analysis procedures.

Address correspondence to Dr Andreas A. Ioannides, Laboratory for Human Brain Dynamics, RIKEN Brain Science Institute (BSI), 2-1

Hirosawa, Wako-shi, Saitama 351-0198, Japan. Email: ioannides@postman.riken.go.jp.

## Supplementary Material

Supplementary material can be found at: http://cercor.oupjournals.org/

## References


Aage R, Moller R, Perte J, Burgess J (1986) Neural generators of the somatosensory evoked potentials: recording from the cuneate nucleus in man and monkeys. Electroencephalogr Clin Neurophysiol 65:241–248.

Benca R, Obermeyer W, Shelton S, Droster J, Kalin N (2000) Effects of amygdala lesions on sleep in rhesus monkeys. Brain Res 879:130–138.

Bodis-Wollner I, Bucher SF, Seelos KC, Paulus W, Reiser M, Oertel WH (1997) Functional MRI mapping of occipital and frontal cortical activity during voluntary and imagined saccades. Neurology 49:416–420.

Braun AR, Balkin TJ, Wesensten NJ, Gwadry F, Carson RE, Varga M, Baldwin P, Belenky G, Herscovitch P (1998) Dissociated pattern of activity in visual cortices and their projections during human rapid eye movement sleep. Science 279:91–95.

Burr DC, Morrone MC, Ross J (1997) Selective suppression of the magnocellular visual pathway during saccadic eye movements. Nature 371:511–513.

Calvo JM, Fernández-Guardiola A (1984) Phasic activity of the basolateral amygdala, cingulate gyrus and hippocampus during REM sleep in the cat. Sleep 7:202–210.

Cespuglio R, Laurent JP, Jouvet M (1975) Etude des relations entre l'activité ponto-geniculo-occipitale (PGO) et la motricité oculaire chez le chat sous réserpine. Brain Res 83:319–335.

Conway BA, Halliday DM, Farmer SF, Shahani U, Maas P, Weir AI, Rosenberg JR (1995) Synchronization between motor cortex and spinal motorneuronal pool during the performance of a maintained motor task in man. J Physiol (Lond) 489:91–924.

Connolly JD, Goodale MA, Menon RS, Munoz DP (2003) Human fMRI evidence for the neural correlates of preparatory set. Nat Neurosci 5:1345–1352.

Datta S, Hobson JA (1994) Neuronal activity in the caudolateral peribrachial pons: relationship to PGO waves and rapid eye movements. J Neurophysiol 71:95–109.

Deboer T, Sanford LD, Ross RJ, Morrison AR (1998) Effects of electrical stimulation in the amygdala on ponto-geniculo-occipital waves in rats. Brain Res 793:305–310.

Fernandez G, Effern A, Grunwald T, Pezer N, Lehnertz K, Dumpelmann M, Van Roost D, Elger CE (1999) Real-time tracking of memory formation in the human rhinal cortex and hippocampus. Science 285:1582–1585.

Funahashi S, Bruce, CJ, Goldman-Rakic, PS (1991) Neuronal activity related to saccadic eye movements in the monkey's dorsolateral prefrontal cortex. J Neurophysiol 65:1464–1483.

Gillin JC, Borbély AA (1985) Sleep: a neurological window on affective disorders. Trends Neurosci 8:537–542.

Gross J, Tass P, Salenius S, Hari R, Freund H-J, Schnitzler A (2000) Cortico-muscular synchronization during isometric muscle contraction in humans as revealed by magnetoencephalography. J Physiol (Lond) 527:623–631.

Halgren E, Walter RD, Cherlow DG, Crandall PH (1978) Mental phenomena evoked by electrical stimulation of the human hippocampal formation and amygdala. Brain 101:83–117.

Hanes DP, Thompson KG, Schall JD (1995) Relationship of presaccadic activity in frontal eye field and supplementary eye field to saccade initiation in macaque: Poisson spike train analysis. Exp Brain Res 103:85–96.

Hashimoto I, Papuashvili N, Xu C, Okada YC (1996) Neuronal activities from a deep subcortrical structure can be detected magnetically outside the brain in the porcine preparation. Neurosci Lett 206:25–28.

Hobson JA, Stickgold R, Pace-Schott EF (1998) The neuropsychology of REM sleep dreaming. Neuroreport 9:R1–R14.

Hong CC-H, Gillin JC, Dow BM, Wu J, Buchsbaum MS (1995) Localized and lateralized cerebral glucose metabolism associated with eye movements during REM sleep and wakefulness: a positron emission tomography (PET) study. Sleep 18:570–580.

Ioannides AA (2001) Real time human brain function: observations and inferences from single trial analysis of magnetoencephalographic signals. Clin EEG 32:98–111.

Ioannides AA, Bolton JPR, Clarke CJS (1990) Continuous probabilistic solutions to the biomagnetic inverse problem. Inverse Problem 6:523–542.

Ioannides AA, Liu LC, Kwapien J, Drozdz S, Streit M (2000) Coupling of regional activations in a human brain during an object and face affect recognition task. Hum Brain Mapp 11:77–92.

Jacobs BL, McGinty DJ (1971) Amygdala unit activity during sleeping and waking. Exp Neurol 33:1–15.

Jouvet M (1962) Recherches sur les structures nerveuses et les mécanismes responsables des différentes phases du sommeil physiologique. Arch Ital Biol 100:125–206.

Jouvet M, Pellin B, Moulier D (1961) Etude polygraphique des differentes phase du someil au cours des troubles de conscience chronique (comas prolong). Rev Neurol 105:181–186.

Leigh RJ, Zee DS (1999) The neurology of eye movements. 3rd edn, pp. 115–116. New York: Oxford University Press.

Luna B, Thulborn KR, Strojwas MH, McCurtain BJ, Berman RA, Genovese CR, Sweeney JA (1998) Dorsal cortical regions subserving visually guided saccades in humans: an fMRI study. Cereb Cortex, 8:40–47.

Maquet P, Peters J, Aerts J, Delfiore G, Degueldre C, Luxen A, Franck G (1996) Functional neuroanatomy of human rapid-eye-movement sleep and dreaming. Nature 383:163–166.

Moller A, Janetta M, Moller M (1982) Intracranially recorded auditiory nerve response in man. Arch Otolaryngol 108:77–82.

Moradi F, Liu LC, Cheng K, Waggoner RA, Tanaka K, Ioannides AA (2003) Consistent and precise localization of brain activity in human primary visual cortex by MEG and fMRI., Neuroimage 18:595–609.

Moschovakis AK, Highstein SM (1994) The anatomy and physiology of primate neurons that control rapid eye movement. Annu Rev Neurosci 17:465–488.

Nelson JP, McCarley RW, Hobson JA (1983) REM sleep burst neurons, PGO waves, and eye movement information. J Neurophysiol 50:784–797.

Niedermeyer E (1991) Awakening epilepsy ('Aufwach-Epilepsie') revisited. Epilepsy Res 2(Suppl):37–42.

Nofzinger EA, Mintun MA, Wiseman M, Kupfer DJ, Moore RY (1997) Forebrain activation in REM sleep: an FDG PET study. Brain Res 770:192–201.

O'Sullivan EP, Jenkins IH, Henderson L, Kennard C, Brooks DJ (1995) The functional anatomy of remembered saccades: a PET study. Neuroreport 6:2141–2144.

Paré D, Curró-Dossi R, Datta S, Steriade M (1990) Brainstem genesis of reserpine-induced ponto-geniculo-occipital waves: an electrophysiological and morphological investigation. Exp Brain Res 81:533–544.

Peigneux P, Laureys S, Fuchs S, Delbeuck X, Degueldre C, Aerts J, Delfiore G, Luxen A, Maquet P (2001) Generation of rapid eye movements during paradoxical sleep in humans. Neuroimage 14:701–708.

Petit L, Orssaud C, Tzourio N, Crivello F, Berthoz A, Mazoyer B (1996) Functional anatomy of a prelearned sequence of horizontal saccades in humans. J Neurosci 16:3714–3726.

Peterson ND, Henke PG, Hayes Z (2002) Limbic system function and dream content in university students. J Neuropsychiatry Clin Neurosci 14:283–288.

Raz J, Turetsky B, Fein G (1988) Confidence intervals for signal-to-noise ratio when a signal embedded in noise is observed over repeated trials. IEEE Trans Biomed Eng 8:646–649.

Rechtschaffen A, Kales A (1968) A manual of standardised terminology, techniques and scoring system for sleep stages of human subjects. Bethesda, MD: US Dept of H and M Neurological Information Network.

Sastre JP, Buda C, Lin JS, Jouvet M., (2000) Differential c-fos expression in the rhinecephalon and striatum after enhanced sleep–wake states in the cat. Eur J Neurosci 12:1397–1410.

Schall JD (1991) Neuronal activity related to visually guided saccades in the frontal eye field of rhesus monkeys: comparison with supplementary eye field. J Neurophysiol 66:559–579.
Schall JD, Thompson KG (1999) Neural selection and control of visually guided eye movements. Annu Rev Neurosci 22:241–259.
Schenck CH, Mahowald MW, Kim SW, O'Connor KA, Hurwitz TD (1992) Prominent eye movements during NREM and REM sleep behavior disorder associated with fluoxetine treatment of depression and obsessive–compulsive disorder. Sleep 15:226–235.
Schlag-Rey M, Amador N, Sánchez H, Schlag J (1997) Antisaccade performance predicted by neuronal activity in the supplementary eye field. Nature 390:398–401.
Segraves MA, Park K (1993) The relationship of monkey frontal eye field to saccade dynamics. J Neurophysiol 69:1880–1889.
Stickgold R (2002) EMDR: a putative neurobiological mechanism of action. J Clin Psychol 58:61–75.
Stickgold R, Hobson JA, Fosse R, Fosse M (2001) Sleep, learning, and dreams: off-line memory reprocessing. Science 294:1052–1057.
Tachibana N, Shinde A, Ikeda A, Akiguchi I, Kimura J, Shibasaki H (1996) Supplementary motor area seizure resembling sleep disorder. Sleep 19:811–816.
Takahashi K, Atsumi Y (1997) Precise measurement of individual rapid eye movements in REM sleep of humans. Sleep 20:743–752.
Talairach J, Tournoux P (1988) Co-planar stereotaxic atlas of the human brain. New York: Thieme.
Tehovnik EJ, Sommer MA, Chou I-H, Slocum WM, Schiller PH (2000) Eye field in the frontal lobes of primates. Brain Res Rev 32:413–448.
Tesche CD, Karhu J (1997) Somatosensory evoked magnetic fields arising from sources in the human cerebellum. Brain Res 744:23–31.
Vanni-Mercier G, Debilly G (1998) A key role for the caudoventral pontine tegmentum in the simultaneous generation of eye saccades in bursts and associated ponto-geniculo-occipital waves during paradoxical sleep in the cat. Neuroscience 86:571–585.
Williams L, Karakan I, Hursh CJ (1974) EEG of human sleep: clinical applications. New York: John Wiley and Sons.